NURETH14-364

DNS OF TURBULENT CHANNEL FLOW AT Re₇=395, 590 AND Pr=0.01

I. Tiselj

"Jožef Stefan" Institute, Ljubljana, Slovenia

Abstract

The paper presents results of the Direct Numerical Simulation of turbulent channel flow at friction Reynolds numbers 395 and 590 with passive scalar at Prandtl number 0.01, which corresponds to the Prandtl number of liquid sodium. Fluctuating and non-fluctuating temperature boundary conditions are analyzed and compared. Results clearly describe the minor role of the turbulent Prandtl number in the integral wall-to-fluid heat transfer.

Introduction

The first Direct Numerical Simulation (DNS) of the passive scalar transfer in the channel was performed in 1989 by Kim and Moin who added a passive scalar equation to the equations of velocity field and performed the scalar transfer calculations. A heat generation was implemented as a uniform volumetric heating with the walls as the heat sinks. Kasagi et al. in 1992 performed the passive scalar DNS in the channel and assumed that the top and bottom walls of the channel heated the fluid. All these simulations were performed with spectral numerical schemes and at low Reynolds numbers (Re_{τ} =180, and Re_{τ} =150, Kim and Moin, and Kasagi, respectively) and at Prandtl numbers lower around 1.

Simulations at higher Reynolds (up to $Re_{\tau}\sim 1000$) and Prandtl numbers between 0.025 and 25 were later performed by various authors. In the present paper the results are compared with DNS databases of Moser et.al. obtained with spectral schemes [1], Kasagi et. al. [2] (spectral) and Kawamura et. al. [6] (finite differences).

At Prandtl number different than one, one should distinguish between the smallest dissipative scales of the velocity field and the smallest dissipative scales of the temperature field, i.e. between the Kolmogorov and Batchelor scale (Batchelor 1959), respectively. The smallest spatial scales of the temperature field are equal to the Kolmogorov scales at Prandtl number Pr=1, while at lower Prandtl numbers the smallest temperature scales are inversely proportional to the square root of the Prandtl number. The present paper is focused on DNS of heat transfer at Prandtl number Pr=0.01, which roughly corresponds to the Prandtl number of the liquid sodium. Like all other materials, constant Prandtl number is not very accurate assumption and Prandtl numbers in liquid sodium reactors vary between 0.004 and 0.01 (see Table 1 for Prandtl number of liquid sodium as a function of temperature). However, the main purpose of the simulations is to produce a database that will be useful for verification of LES and RANS models of turbulent heat transfer at higher Reynolds

number and in realistic geometries, where DNS cannot be performed. Simulations were performed at friction Reynolds numbers 395 and 590 and were foreseen as a part of THINS (Thermal Hydraulics of Innovative Nuclear Systems) project of the 7th research program of European Union, dealing with thermal-hydraulics of sodium cooled reactors.

	density	dynamic	thermal	heat capacity	Prandtl
T (K)	(kg/m^3)	viscosity	conductivity	$c_p (J/kg K)$	number
		*10 ⁻⁴ (Pa s)	(W/mK)		
371	919 (at 400 K)	6.88	89.44	1383.	0.0106
500	897	4.15	80.09	1334.	0.0069
700	852	2.64	68.00	1277.	0.0050
1000	781	1.81	54.24	1252.	0.0042
stainless					thermal
steel					activity ratio K
	~7800		10-20	~500	~0.8-1.6

Table 1: Selected physical properties of liquid sodium [5] and stainless steel.

Heat transfer coefficient in the fully developed turbulent channel flow bounded with walls heated with constant heat flux, is known to be a function of Reynolds and Prandtl number (if the temperature is assumed to be a passive scalar). It is known (Tiselj et.al. [4]) that heat transfer rates near the wall of fully developed turbulent channel flow shows also a weak dependence on the different thermal activity ratios $K = \sqrt{(\rho_f c_{pf} \lambda_f)/(\rho_w c_{pw} \lambda_w)}$ (Table 1). These differences are small, nevertheless they might be relevant for liquid sodium coolant systems. Main differences between isoflux ($K=\infty$) and isothermal (K=0) boundary conditions for dimensionless temperature, which are shown also in the present work, are seen in temperature fluctuations at the wall. While the thermal activity ratio for water and gas flows is usually close to K=0 case, which means no temperature fluctuations at the wall, the turbulent heat transfer between liquid sodium and steel wall is somewhere in between both limiting cases and might be relevant in practice.

1. Mathematical model

A channel is one of the simplest geometry for the near wall turbulent flow studies and as such frequently used for very accurate numerical simulations. The top and the bottom walls are heated by a constant heat source, while the pressure gradient drives the fluid flow in the stream wise direction (x). The flow in the channel is assumed to be fully developed. The following system of Navier-Stokes equations in dimensionless form, also found in the papers of Kasagi et al. 1992 [3] or Kawamura et al. 1998 [6], is used:

$$\nabla \cdot \vec{u}^{+} = 0 \quad , \tag{1}$$

$$\frac{\partial \vec{u}^{+}}{\partial t} = -\nabla \cdot \left(\vec{u}^{+} \vec{u}^{+} \right) + \frac{1}{\text{Re}_{\tau}} \nabla^{2} \vec{u}^{+} - \nabla p + \vec{l}_{x} \quad , \tag{2}$$

$$\frac{\partial \theta^+}{\partial t} = -\nabla \cdot \left(\vec{u}^+ \theta^+ \right) + \frac{1}{\text{Re}_{-} \text{Pr}} \nabla^2 \theta^+ + \frac{u_x^+}{u_y^+} \qquad (3)$$

Term \bar{l}_x (unit vector in the stream wise direction) in equation (2) represents constant dimensionless pressure gradient that drives the flow in the stream wise direction, while only the pressure oscillations are kept in the variable p. Term u_x^*/u_b^* in the equation (3) represents constant dimensionless temperature gradient in the stream wise direction, due to the constant heating of the flow. This temperature gradient is not included into the dimensionless temperature θ^* . Terms \bar{l}_x in equation (2) and u_x^*/u_b^* in equation (3) allow implementation of the periodic boundary conditions in the stream wise and span wise directions. No-slip boundary condition is applied at the wall-fluid interface, while non-fluctuating temperature boundary condition $(\theta^+(y=y_w)=0)$ or fluctuating temperature boundary condition ($\theta^+(y=y_w)=0$) or fluctuations: $d\theta^{*+}/dy(y=y_w)=0$) is applied for the dimensionless temperature θ^+ at the walls. As can be seen from equations (1) to (3), the temperature is assumed to be a passive scalar and does not affect the velocity field. That means that one flow field simulation can be used for parallel simulations with different thermal fields with different Prandtl numbers or with different boundary conditions.

Run	Re_		Grid N _x xN _y xN _z	Grid spacing			Time step	Averaging time
				Δx^{+}	Δy^{+}	Δz^{+}	Δt^{+}	t ⁺
Tiselj	395	2π*2*π	256x257x256	9.69	0.030-4.85	4.85	0.0158	7426
Tiselj	590	2π*2*π	384x257x384	9.65	0.044-7.24	4.52	0.01947	9346
Moser	395	2π*2*π	256x257x256	9.69	0.030-4.85	4.85	/	/
Moser	590	2π*2*π	384x257x384	9.65	0.044-7.24	4.52	/	/
Kasagi	400	2.5π*2*π	192x257x192	16.4	0.030-4.85	6.54	/	47364
Kawamura	395	12.8*2*6.4	512x192x512	9.88	0.300-6.52	4.94	/	14220

Table 2: DNS simulations overview. All simulations were performed with various spectral schemes, except the one by Kawamura performed with 4th-order-space/2nd-order-time accurate finite difference scheme.

The numerical procedure and the code of Gavrilakis et al. [10] modified by Lam [11] and Lam and Banerjee [12] are used to solve the continuity and momentum equations. The code is based on a pseudo-spectral scheme using Fourier series in the stream wise (x) and the span wise (z) directions and Chebyshev polynomials in the wall-normal direction y. The code was later upgraded with an energy equation and improved to solve several energy equations with different boundary conditions and different Prandtl numbers parallel with a single velocity field solution by Tiselj et al. [9]. The solution is advanced in time with second-order accurate Adams-Bashfort algorithm for the nonlinear convective terms and the semi-implicit Crank-Nicholson algorithm for the diffusive terms. Aliasing error is removed with computation of the nonlinear terms on 1.5 finer grid in each direction.

Dimensions of the computational domain and number of Fourier/Chebyshev modes in simulations are identical to the simulation of Moser et. al. who performed the first flow field DNS simulations of that type and are collected in the Table 2 together with some other relevant information. Comparison of various DNS results (Moser et. al. [1], Kawamura et. al [6], Kasagi et. al [3]) performed at the same Reynolds number give an insight into the statistical uncertainties of various DNS databases that are, although very small, important for researchers that use these databases in their work.

2. Results - velocity field

The velocity profiles of various DNS simulations shown in Fig. 1 cannot be distinguished at given resolution of the figure. As shown in Table 3. relative differences in mean velocities between various spectral DNS simulations are less than 1%, while a differences of about 2% can be observed between the spectral data and data obtained by finite differences (FD). Even higher order FD schemes are considered to be less accurate than spectral schemes. Thus finer grids should be applied for finite difference DNS simulations, which is not the case for the FD simulation of Kawamura. Nevertheless, Kawamura DNS database offers other FD DNS results obtained at the same Reynolds number but on different grids and computational domains. Parameters observed in the Tables 3 and 4 and not specified here in detail, vary for ~2% between the various FD DNS computations. It is important to emphasize that spectral schemes behind the DNS data given in Tables 3 and 4 are not the same. All these spectral codes use slightly different algorithms, especially time advancement, where our scheme is the least accurate (2nd-order) and thus requires smaller time steps to obtain the same accuracy of the results as DNS codes of Moser and Kasagi.

Figure 2 shows another variable - streamwise power spectra of the streamwise velocity component and of the pressure fluctuations at the distance y^+ =200 from the wall. Again both spectral DNS results show very similar spectra, while the spectra of the finite difference DNS predicts much stronger dissipation of the higher wave numbers. There are discrepancies visible at high wave numbers also in the results of different spectral codes, however, the exact reason for these is not known.

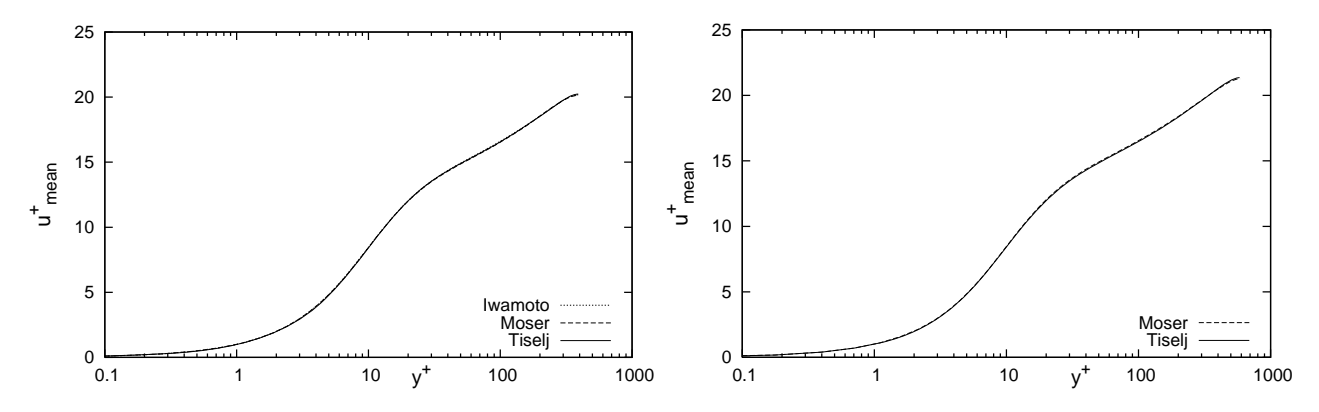


Figure 1 Mean velocity profiles at $Re_T=395$ (left) and $Re_T=590$ (right).

Figures 1 and 2 and Tables 3 and 4 points to the typical uncertainty of the simulations, that are today widely recognized as DNS simulations. From the selected results one can conclude that typical

uncertainty of the main DNS results selected in tables 3 and 4, when computed with higher order finite difference, should not be much larger than $\sim 2\%$.

	Tiselj		Iwamoto, Kasagi		Max. relative difference
u_{RMS}	2.716	2.739	2.721	2.739	0.8 %
V _{RMS}	0.999	0.997	0.996	0.997	0.3%
W _{RMS}	1.293	1.289	1.300	1.301	1.0%
ucenter	20.214	20.133	20.184	20.627	2.4%

Table 3: Comparison of selected parameters of DNS simulations at Re_T=395 (Kawamura simulation: Poi395 4th C.dat).

	Tiselj	Moser	Max.
			relative
			difference
u _{RMS}	2.762	2.774	0.4 %
V _{RMS}	1.042	1.038	0.4%
W _{RMS}	1.371	1.374	0.2%
u _{center}	21.36	21.26	0.5%

Table 4: Comparison of selected parameters of DNS simulations at Re_T=590.

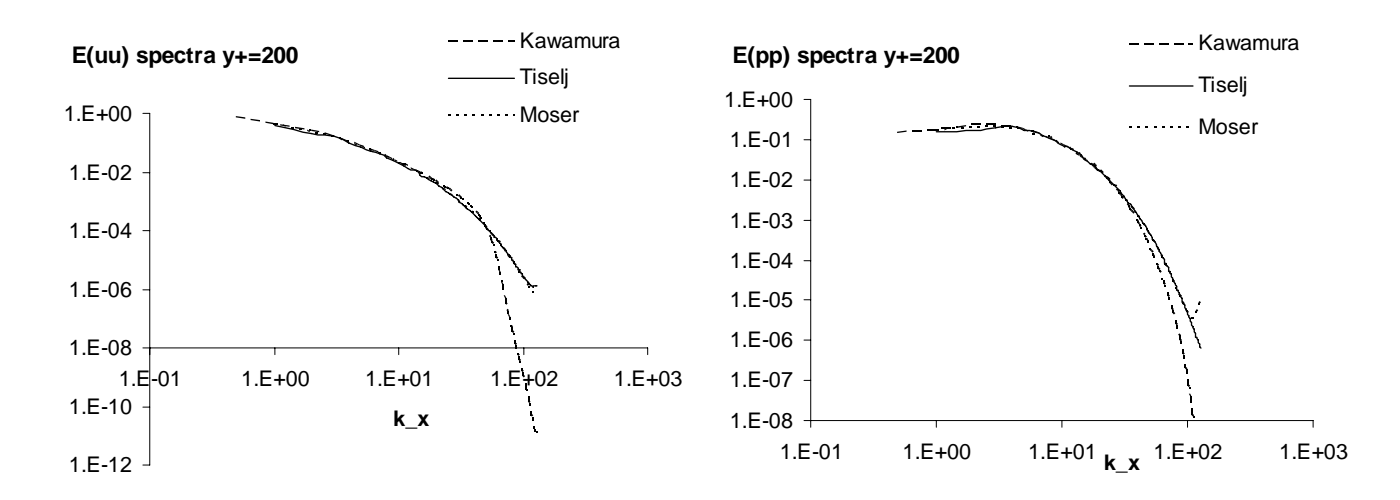


Figure 2 Comparison of streamwise power spectra of streamwise velocity (left) and pressure (right) at Re_T=395 at distance y^+ =200 from the wall. Spectral vs. finite difference schemes.

3. Results - thermal fields

Thermal fields at Pr=0.01 represent an original contribution of the present paper. They give an insight into the mechanisms of the wall heat transfer at low Prandtl number. Mean temperature profiles given in Fig. 3 show two temperature profiles at each Reynolds number: Higher DNS temperature profile belongs to thermal field calculated with non-fluctuating temperature boundary condition and the lower one is temperature profile of the thermal field with fluctuating wall temperature boundary condition. Another temperature profile denoted as "approximate analytic" solution is obtained from Eq. (3) with neglected temporal derivative and neglected convective term. This temperature profile was obtained as solution of 1D ordinary differential equation, that follows from Eq. (3) after neglecting temporal derivative and neglected convective term and taking into account only the mean velocity profile in the u_x^+/u_B^+ term. The "approximate analytic" curves show the dominant role of the heat diffusion comparing to the turbulent heat fluxes.

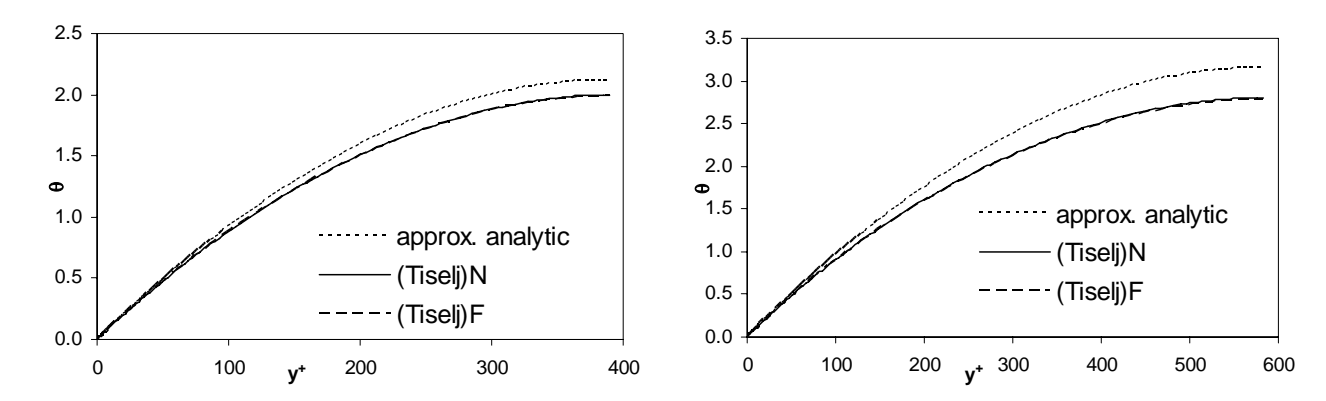


Figure 3 Mean temperature profiles at Re_T=395 (left) and Re_T=590 (right) at Pr=0.01.

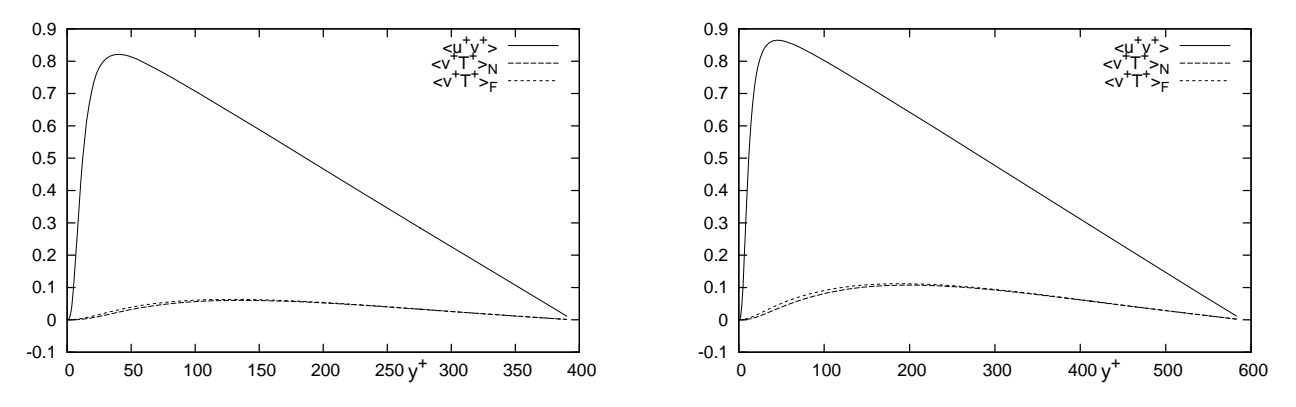


Figure 4 Turbulent heat fluxes and Reynolds stress at Re_T=395 (left) and Re_T=590 (right) for fluctuating (F) and non-fluctuating (N) wall boundary condition at Pr=0.01.

Wall normal turbulent heat fluxes are shown in Fig. 4 compared with the corresponding component of the Reynolds stress. Due to the low Prandtl number, wall normal turbulent heat fluxes are much lower than the corresponding Reynolds stress component. As expected, turbulent heat flux is increasing with the increase of Reynolds number.

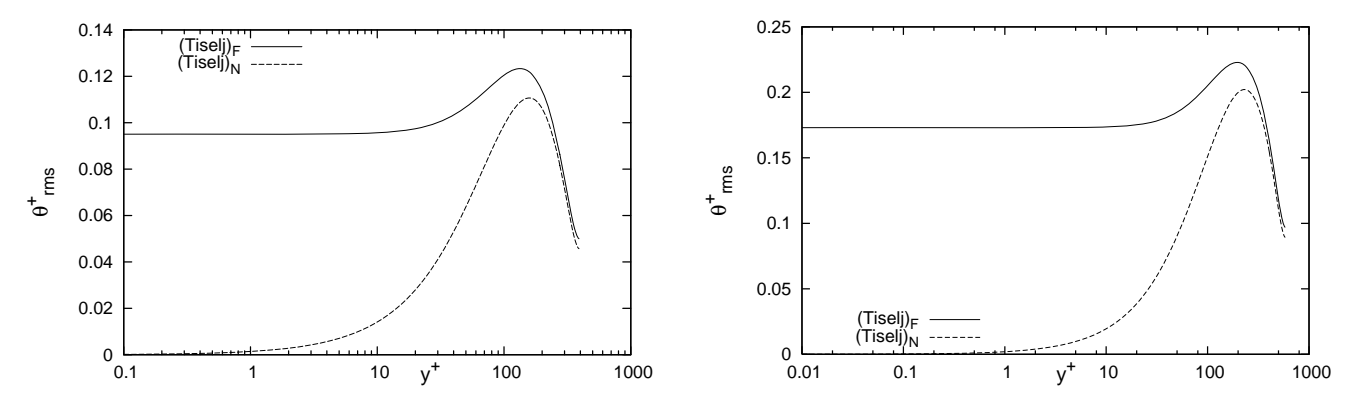


Figure 5 Temperature RMS fluctuations profiles at Re_T=395 (left) and Re_T=590 (right) for fluctuating and non-fluctuating wall boundary condition at Pr=0.01.

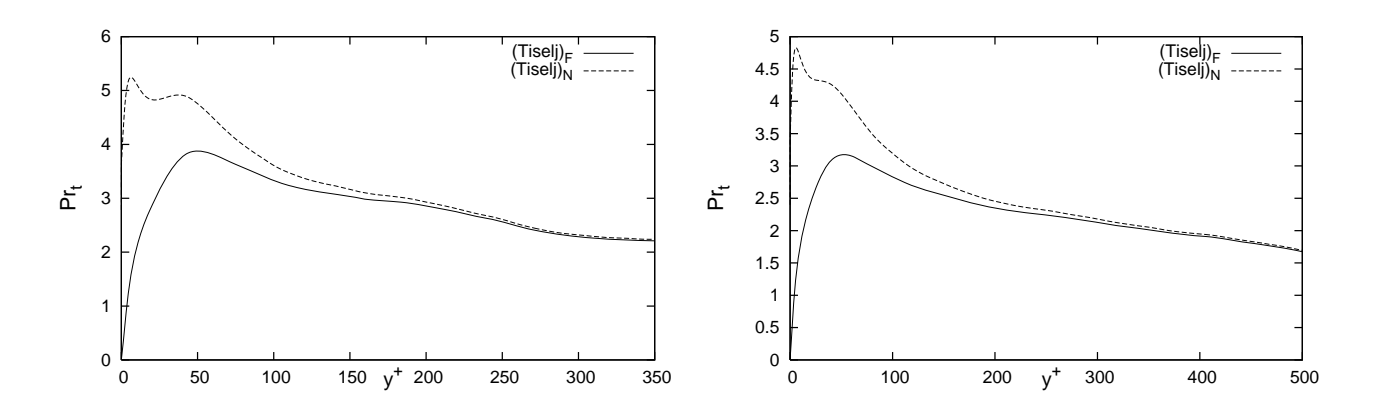


Figure 6 Turbulent Prandtl number profile at $Re_T=395$ (left) and $Re_T=590$ (right). Turbulent Prandtl number at $y^+=0$ for non-fluctuating BC is 3.6 and 3.4 for $Re_T=395$ and $Re_T=590$, respectively.

Figure 5 shows RMS temperature fluctuations in the fluid for two different thermal boundary conditions. These profiles show the main difference between fluctuating and non-fluctuating temperature boundary conditions. Temperature field calculated with non-fluctuating temperature boundary condition does not show any temperature fluctuations at the wall. In experiments, this type of boundary condition appears for most heated walls cooled by air and water. Thermal activity ratio $K = \sqrt{(\rho_f c_{pf} \lambda_f)/(\rho_w c_{pw} \lambda_w)}$, which combines thermal properties of wall material and fluid, is close to zero for such flows. If the thermal activity ratio is high (>10) the system is closer to the fluctuating temperature boundary condition: temperature fluctuations at the wall are not zero and propagate also into the solid wall. As shown in Table 1, thermal activity ratio of sodium/steel

system is around 1, which means roughly half of the wall temperature oscillations seen in Figure 5 for fluctuating temperature boundary condition.

Beside the high thermal activity ratio, fluctuating temperature boundary conditions can be obtained also for very thin heated walls. First comparison of both thermal boundary conditions obtained with DNS is described in [9]. Combination of wall thickness and thermal activity ratios are analysed DNS that includes conjugate heat transfer [8], where detailed form of equations is given also for the solid wall.

Significant differences between both types of thermal boundary conditions are seen also in some other turbulence statistics. Figure 6 shows turbulent Prandtl number profiles, which exhibit significant differences in the near wall region. Turbulent Prandtl number at the wall is zero for fluctuating boundary condition, but retains non-zero values for non-fluctuating boundary condition. Nevertheless, almost invisible differences in the mean temperature profiles of both thermal boundary conditions shown in Fig. 3 mean, that details of the near-wall turbulent heat transfer are not important for the integral heat transfer rate. Thus, turbulent Prandtl number profile in the vicinity of the wall, which is often used in turbulence models of CFD codes, is irrelevant for integral heat transfer rate and can be easily taken as a constant at small Prandtl numbers.

4. Conclusion

The first part of the present paper compares results of the DNS performed with the spectral scheme for the turbulent channel flow at friction Reynolds numbers 395 and 590. Main parameters of the new DNS data show agreement with existing DNS data obtained with spectral schemes within 1%. Larger differences in velocity profiles and RMS velocities of up to 2% can be seen between the spectral schemes and the finite difference DNS data.

The second part of the paper is discussing simulations of passive scalar field with two different boundary conditions: fluctuating and non-fluctuating wall-temperature boundary conditions. While the temperature fluctuations and the turbulent Prandtl number profiles show very large differences in the near wall region, these differences do not have any significant influence on the integral heat transfer between the wall and the fluid. In other words, mean temperature profiles obtained with different thermal boundary conditions are almost identical.

DNS data described in this paper are available to everyone. Please send an Email and request the data from iztok.tiselj@ijs.si.

5. References

- [1] D.R. Moser J. Kim N.N. Mansour, Direct Numerical Simulation of Turbulent Channel Flow up to Re_T=590, Phys. Fluids 11 (4), pp.: 943-945 (1999).
- [2] H. Kawamura, H. Abe, Y. Matsuo, "DNS of Turbulent Heat Transfer in Channel Flow with Respect to Reynolds and Prandtl Number Effects", Int. J. Heat Fluid Fl. 20, 1999, pp. 196.

- [3] N. Kasagi, Y. Tomita, A. Kuroda, "Direct Numerical Simulation of Passive Scalar Field in a Turbulent Channel Flow", J. Heat Trans.-T. ASME 114, 1992, pp. 598.
- [4] I. Tiselj, A. Horvat, B. Mavko, E. Pogrebnyak, A. Mosyak, G. Hetsroni, Wall properties and heat transfer in near wall turbulent flow, Numerical Heat Transfer A 46, 2004, pp.: 717-729.
- [5] J. K. Fink and L. Leibowitz,, A Consistent Assessment of the Thermophysical Properties of Sodium, High Temperature and Materials Science Vol. 35, 1996, pp. 65-103. http://www.insc.anl.gov/matprop/sodium/
- [6] Kawamura, H., Ohsaka, K, Abe, H., Yamamoto, K., 1998, DNS of Turbulent Heat Transfer in Channel Flow with low to medium-high Prandtl number fluid, Int. J. Heat and Fluid Flow 19, pp.: 482-491.
- [7] Kawamura, H., DNS database of turbulent heat transfer http://murasun.me.noda.tus.ac.jp/db/
- [8] I. Tiselj, R. Bergant, B. Mavko, I. Bajsić, G. Hetsroni, DNS of turbulent heat transfer in channel flow with heat conduction in the wall, J. Heat Transfer Transactions of ASME 123 (5), 2001, pp.: 849-857.
- [9] I. Tiselj, E. Pogrebnyak, C.F. Li, A. Mosyak, G. Hetsroni, Effect of wall boundary condition on scalar transfer in a fully developed turbulent flume, Phys. Fluids 13, 2001, pp.: 1028-1039.
- [10] S. Gavrilakis, H.M. Tsai, P.R.. Voke, D.C. Leslie, Direct and Large Eddy Simulation of Turbulence, Notes on Numerical Fluid Mechanics 15, 1986, pp.: 105-112.
- [11] K.L. Lam, Numerical Investigation of Turbulent Flow Bounded by Wall and a Free Slip Surface, Thesis, University of California, Santa Barbara (1989).
- [12] K.L. Lam, S. Banerjee, Investigation of Turbulent Flow Bounded by a Wall and a Free Surface, Fundamentals of Gas-Liquid Flows 72, 1988, pp.: 29-38.

Acknowledgements

This research was financially supported by the Ministry of Higher Education, Science and Technology, Republic of Slovenia, Research program P2-0026 and research project of the EU 7th FP - THINS.